Virginia Commonwealth University
VCU Scholars Compass

Theses and Dissertations | Graduate School

2010

Local Charging Behavior on GaN Surfaces

Josephus Ferguson
Virginia Commonwealth University

Follow this and additional works at: https://scholarscompass.vcu.edu/etd

 Part of the Physics Commons

© The Author

Downloaded from
https://scholarscompass.vcu.edu/etd/82

This Thesis is brought to you for free and open access by the Graduate School at VCU Scholars Compass. It has been accepted for inclusion in Theses and Dissertations by an authorized administrator of VCU Scholars Compass. For more information, please contact libcompass@vcu.edu.

www.manaraa.com

Local Charging Behavior on GaN surfaces

A thesis submitted in partial fulfillment of the requirements for the degree of Master of Science in Physics / Applied Physics at Virginia Commonwealth University.

By

Josephus Ferguson

B.S. in Physics and Applied Mathematics

Virginia Commonwealth University, 2008

M.S. in Physics/Applied Physics

Virginia Commonwealth University, 2010

Directors:

Alison. A. Baski, Associate Professor, Department of Physics

Mikhail A. Reshchikov, Associate Professor, Department of Physics

Virginia Commonwealth University

Richmond, Virginia, 23284

April 25, 2010

www.manaraa.com

Acknowledgments

First and foremost, I would like to thank my parents and family, who have made me the person who I am today. Their help and support has been tremendous, and I can't thank them enough for all of their love and guidance.

Secondly, this work could not have been accomplished without the support of the VCU Physics Department. Sincere thanks are in order to the professors who have inspired and educated, to the caring administration who always cheer me up, and to my fellow students, who always lend helping hands and minds. A special thanks to Dr. Alison Baski, Dr. Michael Reshchikov, and those in the Baski/Reshchikov research group who have helped with the studies that are included within this thesis, including some figures in this report, which were taken by Michael Foussekis; I thank him for his contributions.

Many more at VCU deserve thanks as well. The resources and support that VCU has offered has been remarkable, and it has been an absolute treat to be part of a rapidly maturing institution that shows more promise and improvement every day.

A special thanks to Dr. Dmitry Pestov of the Mechanical Engineering Department for XPS survey data and oversight of the Nanomaterials Characterization Center at VCU. The Hadis Morkoç group and the Virginia Microelectronics Center at VCU were also instrumental in sample preparation and collaborative efforts with our research group.

Lastly, I'd like to thank you, the reader, for showing an interest. May you enjoy this report.

www.manaraa.com

Table of Contents

www.manaraa.com

List of Figures

www.manaraa.com

www.manaraa.com

Abstract

Local Charging Behavior on GaN surfaces

By Josephus D. Ferguson III

A thesis submitted in partial fulfillment of the requirements of the degree of Master of Science at Virginia Commonwealth University. Virginia Commonwealth University, 2010.

Major Director: Dr. Alison A. Baski, Chair, Department of Physics

Gallium nitride is an important III-V semiconductor which is used in many optoelectronic and high-frequency devices. The nature of the GaN surface and its electrical characteristics can impact the performance of such devices. In this study, several GaN surfaces are locally charged using an atomic force microscope, and then subsequently studied by measuring the surface potential with scanning Kelvin probe microscopy (SKPM). The charging and discharging behavior of the surface appears to be strongly influenced by surface preparation and the presence of a surface oxide layer. If a substantial oxide layer exists, then both positive and negative charging is possible on n-type and p-type samples. Surface treatments and photoemission spectroscopy (XPS) data confirm the presence and influence of the oxide layer on surface charging behavior. In the case of forward-bias charging, a small change in surface contact potential (0.1 – 0.3 eV) is observed that is primarily due to a small voltage drop across the surface oxide. Reverse-bias charging produces a substantially larger change in surface potential (~1 – 3 eV) that must be explained by a large increase in surface band bending. Temperature-dependent SKPM measurements also indicate that the decay behavior of deposited surface charge in dark involves a thermionic mechanism.

www.manaraa.com

Chapter 1: GaN and Scanning Probe Techniques

1.1 Motivation

GaN is an important III-V semiconductor material in present-day optoelectronic devices. Its wide, direct bandgap of 3.4 eV is favorable for many applications, and its crystalline properties give GaN high structural stability.[1] It is currently used for UV laser diodes, including Blu-Ray™ technology, which can write and read data at much higher densities than the red-light laser diodes found in traditional CD and DVD drives. Because of its wide bandgap and correspondingly short wavelength light, GaN laser diodes can read and write optical data at a higher storage density.[1] The readable "spot size" of 580 nm for Blu-Ray optical devices, compared to the spot size of at least 850 nm for red-light optical lasers, illustrates the higher efficiency of large-bandgap GaN laser diodes.

Presently, GaN-based LEDs which allow for near-white color rendition can be produced, through the use of either yttrium aluminum garnet (YAG)-based or phosphor-based fluorescent coatings on the inside of LED bulbs. The coating is necessary since the coating material typically re-emits high-energy UV GaN photons as longer, visible wavelength light (Stokes fluorescence). GaN-based LED lights, however, only consume a fraction of the electrical power that an incandescent light bulb of similar light intensity would consume. Clearly, these LEDs are of interest, particularly for use in low power, high-efficiency lighting applications. GaN devices also show potential widespread use in high-frequency switching and power amplification devices, including radio frequency (RF) transmitters[2]. Because of the high melting point of GaN (>2750 K) and its high thermal conductivity of $1300 Wm^{-1}K^{-1}$ under ambient conditions,[1] GaN is also suitable for high-temperature semiconductor applications.[3]

Despite the present application of GaN in devices, research on the surface behavior and associated electronic properties of GaN is lacking. It is certainly conceivable that accumulation of charge on the GaN surface may play a deleterious role in the proper functioning and intrinsic lifetimes of GaN-based devices.[4] This thesis seeks to explore and

www.manaraa.com

explain some of the interesting surface charge phenomena that exist on the GaN surface using variants of atomic force microscopy (AFM).

In 1986, Gerd Binnig, Calvin Quate, and Christoph Gerber constructed a new type of microscopy tool, known as the atomic force microscope (AFM),[5] which was borne out of the earlier invention of the scanning tunneling microscope (STM) in 1981.[6] The nanoscale imaging capabilities of AFM and the many variants of this technique have been critical in the rapidly expanding area of nanoscience. Many material properties can now be measured, e.g., topography, surface potential, magnetism, and manipulated on the nanometer scale.[7,8]

The AFM technique used in this work to create locally-charged regions on sample surfaces has previously been observed and reported in the literature for insulating surfaces and for n-type GaN surfaces.[9,10] Here, we locally charge both n-type and p-type GaN with both polarities and investigate the resultant discharge behavior.[11,12] In this thesis, Chapter 1 introduces the experimental method and describes the set of GaN samples under investigation. Detailed analysis of the surface charge behavior will be discussed in Chapter 2, while surface treatment effects will be explored in Chapter 3 and the resulting energy band diagrams in Chapter 4.

1.2 Experimental Methods

We use the AFM to both locally charge a GaN surface and then subsequently detect this charge as a change in the local surface potential. For GaN surface charging and subsequent surface potential measurements, two modes of a commercial AFM are employed.[13] The first mode is used for locally charging the surface by operating the AFM in contact-mode while a constant sample-to-tip voltage is applied.[14] Unless otherwise noted, all surface charging scans are 5x5 μm^2 with a scan rate of 1 Hz/line (corresponds to a tip velocity of 10 μm/s). In our experimental setup, the voltage is applied to the sample (V_S) with a magnitude of 10 V. The schematic in Fig. 1.1(a) shows the process of negative surface charging with a sample bias of $V_S = +10V$. This bias polarity should result in the transfer of electrons from the tip to the sample surface, which usually results in a locally charged region with a more negative surface potential. Conversely, positive surface charging with a sample bias of $V_S = -10V$ should result in an increase in surface potential in the scanned region. Thus, we can locally

www.manaraa.com

charge the surface with excess positive or negative charge by scanning with contact-mode AFM using an appropriate bias voltage.

After locally charging the surface, the surface potential in that region is then measured using another mode of AFM known as scanning Kelvin probe microscopy (SKPM).[15] In this technique, a two-step process is used during each scan line. First, the surface topography is acquired using tapping mode AFM and then the tip is lifted above the surface a prescribed "lift" height. A lift height of 80 nm was used in this study to maximize the electrostatic response while minimizing topological convolution.[16] Next, the tip rescans the line at this lift height while following the previously measured topography, thereby minimizing topographical effects. If any change in the surface potential exists during a measurement, the tip will interact with the charge, and a force must be applied to the tip to minimize the electrostatic interaction.[17]

SKPM data is acquired through the application of an AC potential onto the metallized tip, which results in an electrostatic force interaction with the surface charge. For the measurement of the surface potential, the applied external voltage has the form of $V = \left(V_{DC} + V_{AC} \sin \omega t\right)$, where the frequency ω of the AC component is the resonant frequency of the cantilever. The force between the cantilever and the surface is then[18]

$$F = -\frac{\partial U}{\partial z} = -\frac{1}{2}\frac{dC}{dz}V^2,$$

where U is the electrostatic energy, z is the direction normal to the surface, C is the capacitance between the conducting tip and the sample, and the voltage

$$V = -V_{CP} + V_{DC} + V_{AC} \sin \omega t\,.$$

The resultant force has a DC and two AC force components (ω, 2ω) as follows:

$$F = F_{DC} + F_{\omega} + F_{2\omega} = F_0 + F_1 \sin(\omega t) + F_2 \cos(2\omega t)\,.$$

The F_{ω} force is then used for the contact potential V_{CP} measurement, since

$$F_{\omega} = -\frac{dC}{dz}(V_{CP} - V_{DC})V_{AC} \sin\left(\omega t\right).$$

A simplified schematic of a typical SKPM measurement for detection of negative charge placed on a sample surface is shown in Fig 1.1(b).

www.manaraa.com

In our studies, SKPM images are typically acquired using a 20 μm scan width and 512 pixel/line resolution, resulting in a minimum resolution of ~20 nm. However, SKPM has a lower spatial resolution than AFM due to the long-range characteristic of the Coulomb force, increased tip size due to metallization, higher tip velocities, etc.[16,19] In this study, SKPM measurements are always taken with larger scan sizes than the scan sizes used to charge the surfaces in order to accurately measure the difference in potential, ΔV_{CP}, between scanned and unscanned regions. Therefore, for two regions with different V_{CP} values,

$$\Delta V_{CP} = \left(V_{CP1} - V_{CP2}\right).$$

where V_{CP1} is the potential in the scanned region and V_{CP2} is the potential in the unscanned region.

In addition to SKPM imaging, in this work we measure time-resolved SKPM for a single scan line. This allows the observation of time-dependent decay characteristics of charged areas. In this mode, the ΔV_{CP} values from one scan line are repeatedly measured over time by scanning at 0.25 Hz while the y-axis motion is disabled. Therefore, a time-resolved SKPM "image" comprises 512 lines which are each separated in time by 8 s. Typically, we plot the 'normalized' magnitude of ΔV_{CP} ("1" = maximum) vs. time (t = 0 s at time of charging) in order to compare data from different samples. Note that careful attention must be paid to the elapsed time between initial charging and SKPM data acquisition, which is usually ~250 s after initial surface charging.

1.3: Sample Preparation

To compare and contrast the surface charging behavior of GaN, four different samples were used in this study, which included two n-type and two p-type samples (see Table 1). All samples were grown on c-plane sapphire substrates with two different techniques: metal-organic chemical vapor deposition (MOCVD) for one p-type sample (2040) from SUNY-Albany, and hydride vapor-phase epitaxy (HVPE) for the remaining samples from TDI, Inc. The samples should show similar crystalline structure, although the MOCVD p-type sample (2040) contains a thin, degenerate n-type layer at the sapphire/GaN interface. The influence of this degenerate layer on surface behavior should be minimal, but did affect Hall Effect

www.manaraa.com

measurements.[20] In order to make electrical contact to the samples for SKPM measurement, an indium solder contact was placed between the sample surface and specimen disc.

Table 1.1: Description of Samples in this Study

Sample	Doping type	Technique	Source
2015	n-type (Si), $n = 6\times10^{18}$	HVPE	TDI, Inc.
2752	n-type		
1321	p-type (Mg)	HVPE	TDI, Inc.
2040	p-type (Mg) $p = 2\times10^{16}$	MOCVD	Suny-Albany

www.manaraa.com

Chapter 1 Figures

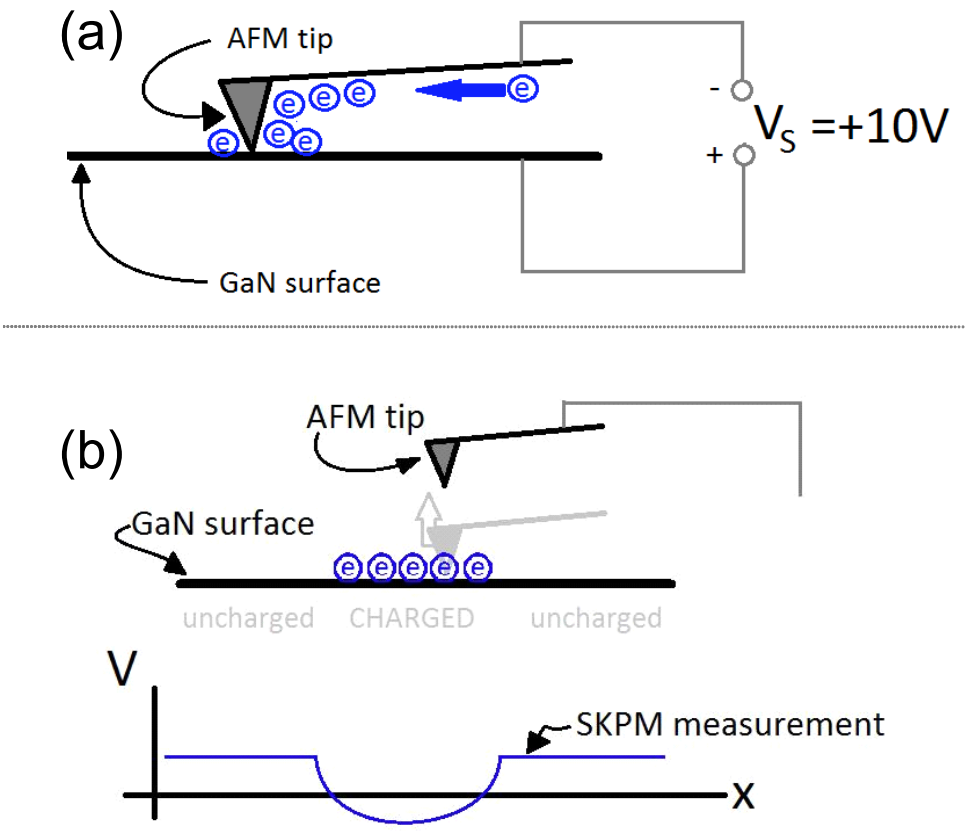

Fig. 1.1: Contact AFM is used to place charge on the surface (a), and resulting surface potential is measured with SKPM (b).

www.manaraa.com

Chapter 2: Local Charge Storage on GaN Surfaces

2.1 Introduction

In this chapter, we will see that both n-type and p-type GaN surfaces can be locally charged using both bias polarities. It appears that charging is more effective under reverse-bias conditions, e.g., negative charging on n-type samples or positive charging on p-type samples. In the case of forward-bias charging, e.g. positive charging on n-type samples, surface charging is only possible after some surface treatment. Exposure of the sample to ambient humidity and/or extended UV light illumination under ambient are two such surface treatments used here. It will also be shown that since the applied charge persists on the surface for an extended period, "erasure" of surface charge can be accomplished by re-scanning over pre-existing charge with the opposite V_S polarity. We also examine the decay behavior of surface charge under dark conditions and observe a logarithmic behavior. It appears that negative surface charge decays at a higher rate than positive charge, and that the decay rate increases with temperature for both positive and negative surface charges.

2.2 Positive and Negative Charging on n-type and p-type GaN Surfaces

In this section, we locally charge n-type and p-type GaN surfaces at both polarities using the technique presented in Chapter 1. The initial charging area and subsequent SKPM scan size may vary somewhat, but relevant scan parameters are presented accordingly. After charge is written to the surface using contact AFM with an applied voltage of ±10 V, SKPM is used to measure the local surface potential to verify the presence of charge.

The charging behaviors at both bias polarities for two n-type samples are shown in Fig. 2.1. The negatively charged areas on the right side of each SKPM image, sample 2752 in Fig. 2.1(a) and sample 2015 in Fig. 2.1(b), were first written in reverse bias with $V_S = +10$ V. It should be noted that a Schottky contact between the metallized AFM tip and sample surface results in a rectifying junction with reverse bias corresponding to a positive voltage applied to the sample. Immediately afterwards, a forward-bias scan using the opposite V_S polarity was performed to the left of the initial scan area to create the positively-charged region. Each charged region represents a 5×5 μm^2 scan with a 1 μm separation between

www.manaraa.com

regions. Cross-sectional data taken at the midlines of the regions are shown below each corresponding image. These data verify the presence of positive and negative charge on the surface, and indicate the ΔV_{CP} values for the magnitude of surface charge. Fig. 2.2 shows similar SKPM data for two p-type samples. Here, sample 2040 (Fig. 2.2a) and sample 1321 (Fig. 2.2b) are both locally charged in the same manner as discussed above. However, since p-type samples contain holes as majority charge carriers, $V_S = -10V$ corresponds to reverse-bias and $V_S = +10V$ to forward-bias conduction. Again, cross-sectional data indicate ΔV_{CP} values for each charged region on the p-type surface.

By comparing Fig. 2.1 and Fig. 2.2, we observe an intrinsic asymmetry between the magnitudes of surface charge on each sample. The data indicate that reverse-bias charging more effectively transfers charge, i.e., n-type samples show larger ΔV_{CP} values for negative charging and p-type samples show larger ΔV_{CP} values for positive charging. In contrast, forward-bias charging results in smaller ΔV_{CP} values for the same applied bias voltage. In fact, for “clean” samples which do not have a substantial surface layer of oxygen species, forward-bias charging scans will not usually produce the expected surface charge when subsequently imaged with SKPM. However, a surface layer of oxygen species may allow some charge transfer, where the residual charge is stored within this surface layer.

An experiment demonstrating how surface treatment can significantly affect forward-bias charging is demonstrated in Fig. 2.3 for an n-type sample. Here, extended exposure to ambient water vapor is used to promote the growth of a surface layer. As shown in Fig. 2.3(a), the as-received surface does not show the expected positive charging for forward-biased scanning. The sample was then placed in a high-humidity (>70% rel. hum.) environment for 3 h in order to promote the growth of a surface layer. Following this treatment, forward-bias conditions resulted in positive charging within the scanned region (Fig. 2.3b). Interestingly, when the surface was wiped with isopropanol and dried under N_2 , this positive charging no longer occurred. In fact, negative charging occurred for forward-bias conditions on this "wiped" n-type sample. Apparently, the alcohol resulted in a surface layer that strongly trapped electrons during charging, regardless of the sample polarity used. These results suggest that an oxygen-rich layer on the GaN surface is necessary to observe

www.manaraa.com

forward-bias charging. Surfaces exposed to high humidity levels for an extended period of time form this necessary layer. This same dependence was observed for forward-bias charging on p-type samples.

2.3: Sequential Charging

The ability to place positive and negative charge on GaN surfaces enables us to erase and pattern surface charges by appropriately changing the charging polarity. Fig 2.4 shows two SKPM images demonstrating this capability on a p-type sample (1321). We can effectively erase positive charge by switching the V_S bias and re-scanning the area. The top SKPM image shows three positively-charged regions with square shape ($V_S = -10$ V, 5x5 μm^2) written in sequence from left to right. The right-most square is brighter with a higher ΔV_{CP} because it has decayed for a shorter time as compared to the other regions. Next, the right-most square was re-scanned using the opposite bias polarity ($V_S = +10$V). The SKPM image taken immediately afterward (Fig. 2.4b) indicates that this procedure effectively "erases" the original charge, and cross-sectional data (Fig 2.4c) show a surface potential nearly equal to the unscanned regions.

In addition to effectively erasing all charge in a region, it is possible to sequentially pattern such charge. Two examples are demonstrated in Fig. 2.5 for both n-type and p-type samples. In Fig. 2.5(a), a positively-charged outer square (5×5 μm^2) was first written in forward bias on an n-type sample with $V_S = -10$V, and then the bias was reversed and the tip was held in contact with the surface for 5 s without scanning. Since this second step involved reverse-bias charging, the area of charge deposition was significant and nearly 50% of the originally charged area was erased. Another example of this sequential patterning is illustrated in Fig. 2.5(b) for a p-type sample. In this case, a positively-charged outer square (5×5 μm^2) was written in reverse bias ($V_S = +10$ V), followed by a rotated square (2.5×2.5 μm^2) written in forward bias ($V_S = -10$ V). Finally, the tip was held in contact with the surface at reverse bias again for 5 s without scanning. The resulting SKPM image shows the expected features, where in this case the last step with the reverse-bias tip contact results in a very small feature. This result is in contrast to the experiment in Fig. 2.5(a) where reverse-bias tip contact resulted in a significantly larger feature. Therefore, positive charging

www.manaraa.com

results in more well-defined features, whereas negative charging demonstrates more lateral diffusion away from the scanned region. These experiments demonstrate that localized charge can be arbitrarily written to GaN surfaces, although with limited spatial resolution between charged features.

2.4: Decay Characteristics of Surface Charge

In order to better understand the rate of diffusion of applied surface charges, decay data was obtained using the time-resolved SKPM method described in Chapter 1. Here, we will see that the decay behavior appears to be logarithmic in time, and that negative surface charge consistently decays at a faster rate than positive surface charge on both types of GaN surfaces. We also verify that an increase of sample temperature facilitates faster decay.

We first compare the decay rate of positive and negative surface charge at room temperature for both n-type and p-type surfaces. Average ΔV_{CP} values are acquired approximately every 8 s and then plotted as a normalized value (maximum $\Delta V_{CP} = 1$) on a logarithmic time scale. Fig. 2.6 illustrates decay data for both positively and negatively charged regions on n-type and p-type samples. In both cases, the negative surface charge decays at a measurably faster rate, suggesting a higher rate of electron transfer from the surface into the bulk (vs. bulk-to-surface for positive charge decay). Interestingly, the n-type surface shows a faster decay for both negative and positive charge, and the negative charge is nearly gone after only 1 h.

Next, we examined the effect of sample temperature on decay rates. Here, data is collected for experimental runs performed at room temperature and at 100º C for n-type (Fig. 2.7a) and p-type (Fig. 2.7b) samples. As expected, sample heating during charging resulted in faster decay rates with a correspondingly increased slope for both types of charge. This behavior indicates that charge decay involves a thermionic charge transfer mechanism, where higher temperatures increase the number of electrons overcoming a near-surface barrier.

It should be noted that the surface charge decay behavior is also influenced by surface treatments. The effect of an oxide grown by extended UV exposure has been observed in surface photovoltage decay behavior as well[12]. Such surface treatment effects will be presented in the following chapter in detail.

www.manaraa.com

Chapter 2 Figures:

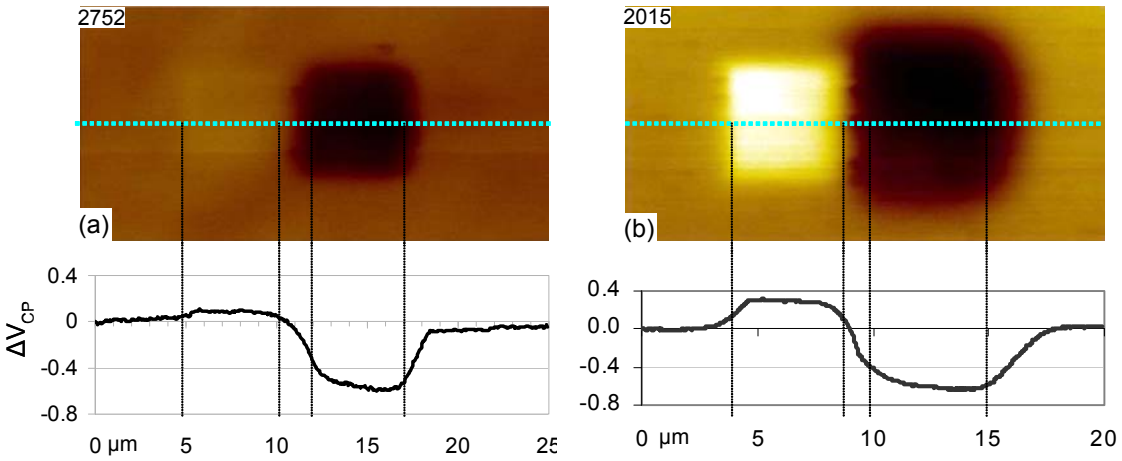

Fig. 2.1: SKPM images of positive and negative surface charging on n-type GaN samples (a) 2752 and (b) 2015. Cross-sectional ΔV_{CP} data at midline (dotted) shown for each image

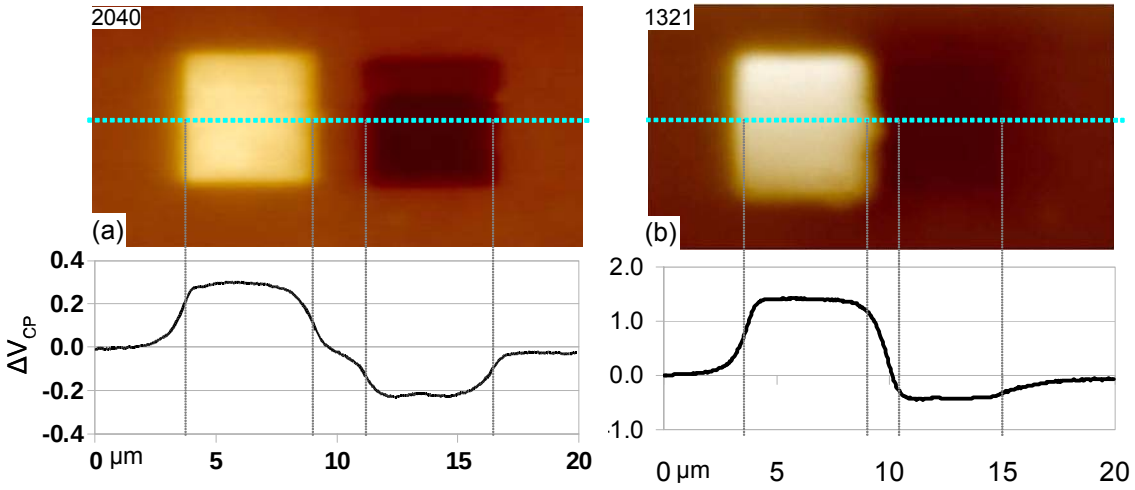

Fig. 2.2: SKPM images of positive and negative surface charging on p-type GaN samples (a) 2040 and (b) 1321. Cross-sectional ΔV_{CP} data at midline (dotted) shown for each image

www.manaraa.com

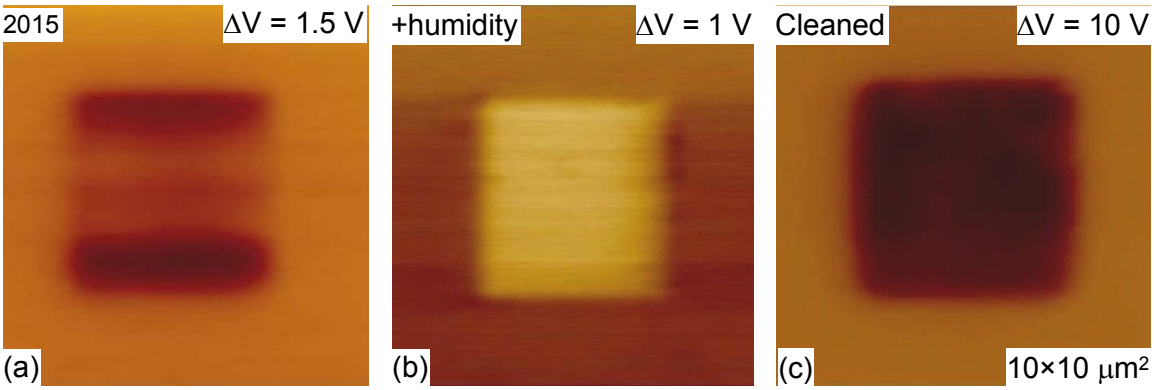

Fig. 2.3: Surface charging behavior for VS = –10 V on an n-type sample. (a) As-received, (b) high humidity conditions, and (c) isopropanol/N2-treated surface.

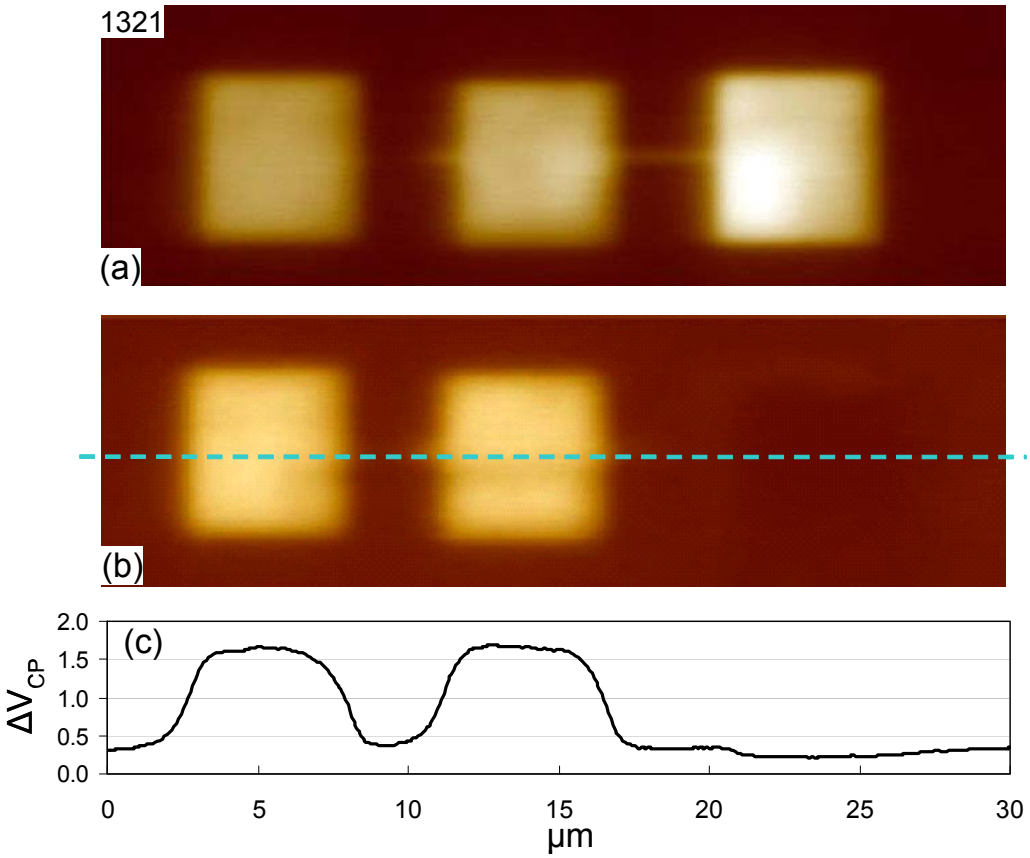

Fig. 2.4: "Erasing" charge on a p-type sample. (a) Three positively-charged regions, (b) same area after right-most square is rescanned at opposite bias, and (c) cross-sectional ΔV_{CP} data for indicated line in (b).

www.manaraa.com

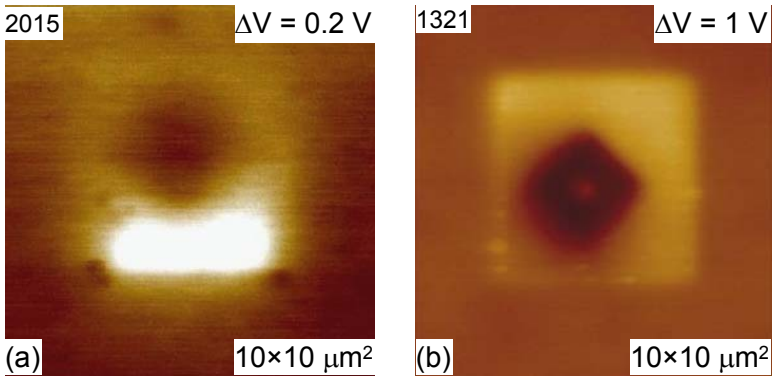

Fig. 2.5: Sequential patterning of charge on (a) n-type sample and (b) p-type sample.

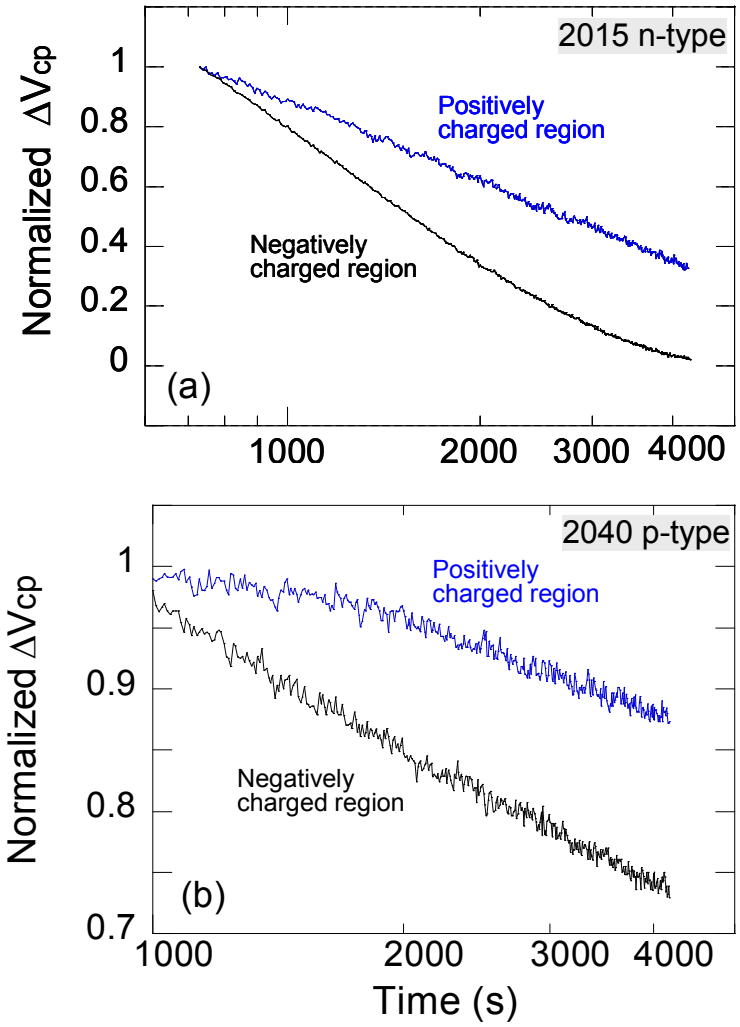

Fig. 2.6: Decay behavior as a function of time for (a) n-type sample and (b) p-type sample.

www.manaraa.com

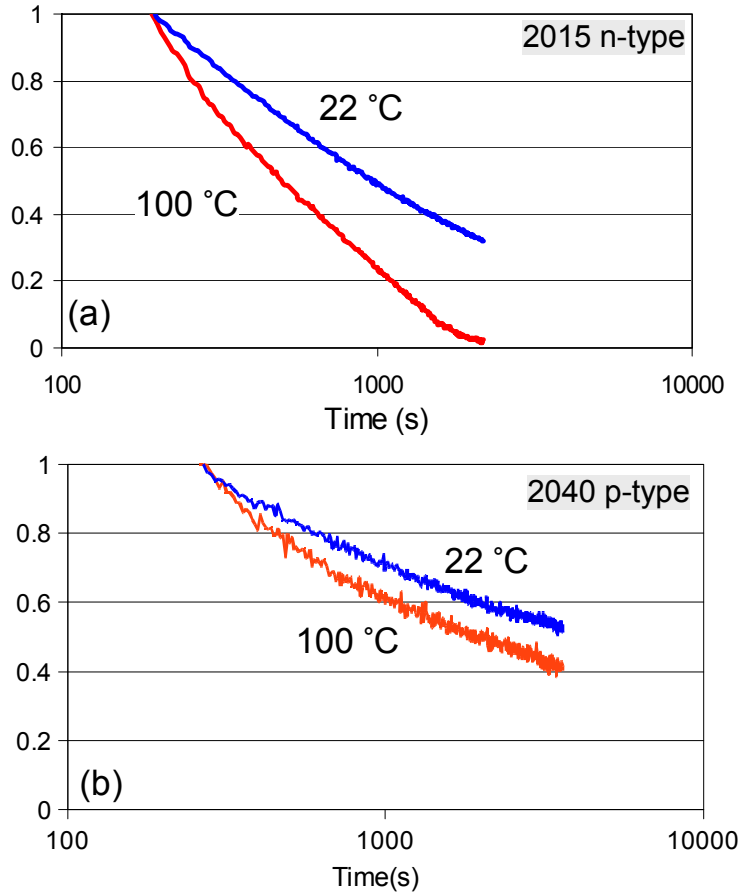

Fig. 2.7: Decay behavior at room temperature and 100 ºC for (a) n-type sample and (b) p-type sample.

www.manaraa.com

Chapter 3: Surface Treatment and Effects on Surface Charging

3.1 Introduction

It was shown in the previous chapter that an adsorbed surface water layer can affect the charging behavior of GaN surfaces. This sensitivity to the environment could potentially affect device performance and we therefore studied the effect of other surface treatments on surface charging. In this chapter, we examine how extended ultraviolet (UV) exposure affects charging for an n-type sample (2015). After several hours exposure to UV light, the surface appears to grow an oxide that causes significant lateral spreading of negative charge. The presence of a UV-grown surface oxide and its removal with aqua regia is confirmed using X-ray photoelectron spectroscopy (XPS).

3.2 UV Surface Treatment and Effect on Charging

As previously mentioned, an oxide may be grown on the surface through exposure to high ambient humidity. Exposure to UV light for extended periods of time in ambient also facilitates the growth of a surface oxide layer,[21] which is separate from the native oxide layer. Here, we compare charging behavior for an as-received and UV-treated surface of an n-type sample (2015). The UV treated sample was placed ~15 cm from a UV source (100-W, Hg bulb) for a period of 100 h. We note here that because the sample was stored in ambient that a native oxide layer was already present on the as-received surface. Negative charging behaviors for the as-received and for UV-treated samples are shown in Fig. 3.1. The cross-sections from both samples show a similar amount of negative charge; however, there is lateral delocalization of the negative charge for the UV-treated sample. This type of lateral "leakage" is not observed for positive surface charging on the UV-treated sample, as shown in Fig. 3.2. Also, the amount of positive charge transferred to the surface is significantly enhanced by UV-treatment. The surface therefore behaves differently for both charging polarities as a result of the UV treatment.

www.manaraa.com

The as-received sample and another UV-treated sample from the same wafer were then examined using x-ray photoemission spectroscopy (XPS) to determine its surface chemical composition. XPS[22] confirms the presence of an oxide on the UV-treated sample. Fig. 4.3 shows data obtained by the XPS surveys for the behavior of the initial and UV-treated surface. For alignment between the surveys (Fig 3.3a), the well-known and stable carbon 1s peak, located at 284.6 eV, was used to correct for charge-shifting between experimental runs.[12] A high-resolution survey of the Ga 3d peak at 19 eV (Fig. 3.3b) shows a ~0.3 eV increase in binding energy and a decrease in peak intensity for the UV-treated sample, consistent with a lower concentration of surface Ga. Conversely, high-resolution data for the O 1s peak (Fig. 3.3c) indicate an increase in surface oxygen for the UV-treated sample. The shift in binding energies of the two peaks indicates a change in the chemical binding environment, suggesting the presence of a grown surface oxide that is distinctly different from the native surface. The effect on surface charging due to the presence of a surface oxide may be further understood by investigation of associated energy band diagrams, where the surface oxide affects the charging behavior of the GaN surface. An overview of band diagrams for different biasing regimes on n-type and p-type samples will be addressed in Chapter 4.

www.manaraa.com

Chapter 3 Figures:

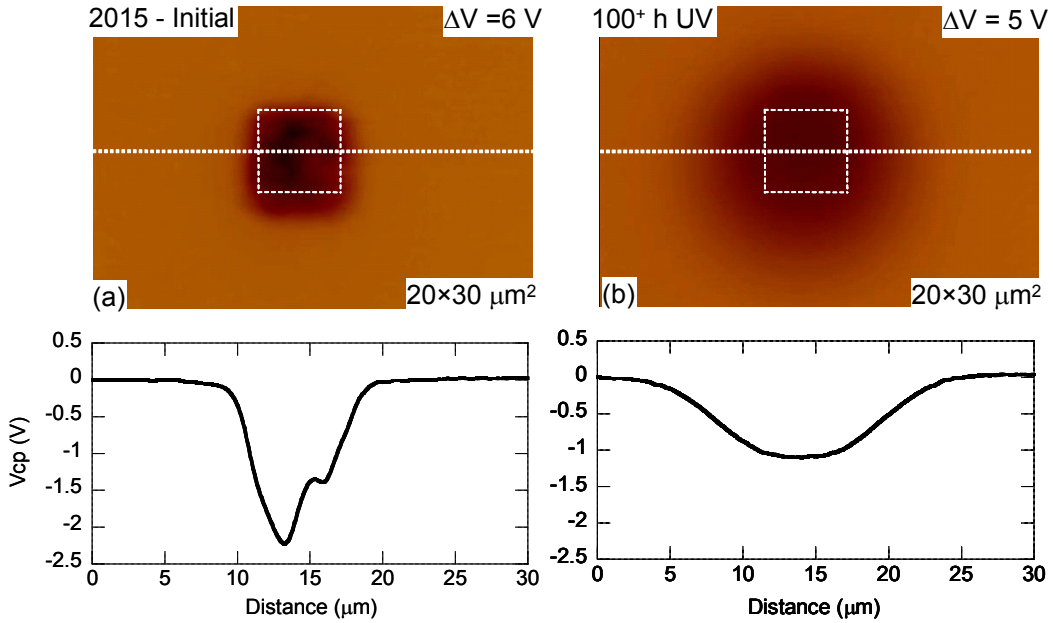

Fig. 3.1: Negative charging on n-type sample for (a) as-received and (b) UV-illuminated surfaces. Cross-sectional ΔV_{CP} data shown below each image.

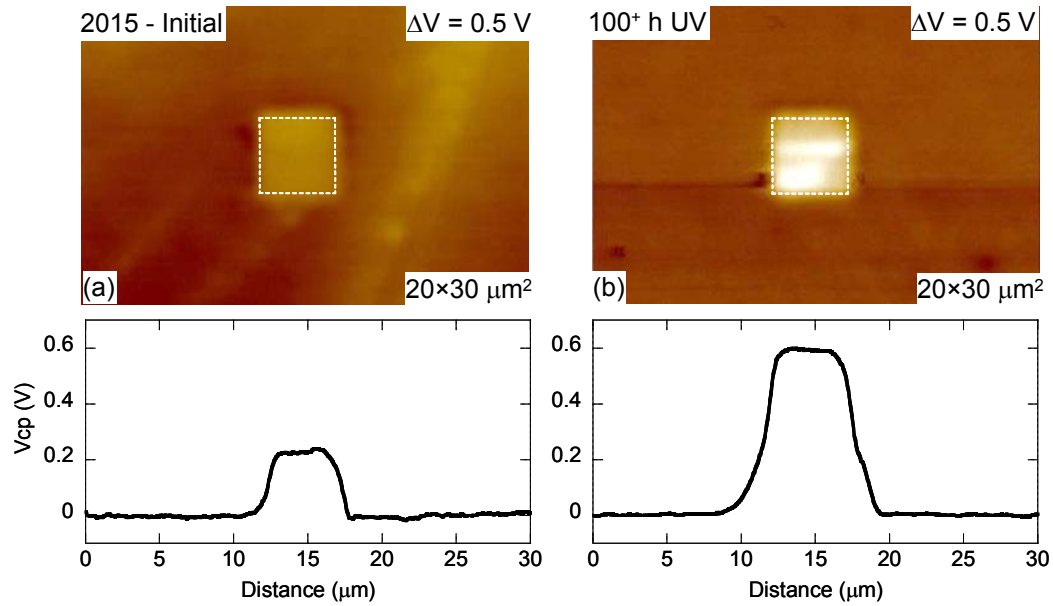

Fig. 3.2: Positive charging on n-type sample for (a) as-received and (b) UV-illuminated surfaces. Representative cross-sectional ΔV_{CP} data shown below each image.

www.manaraa.com

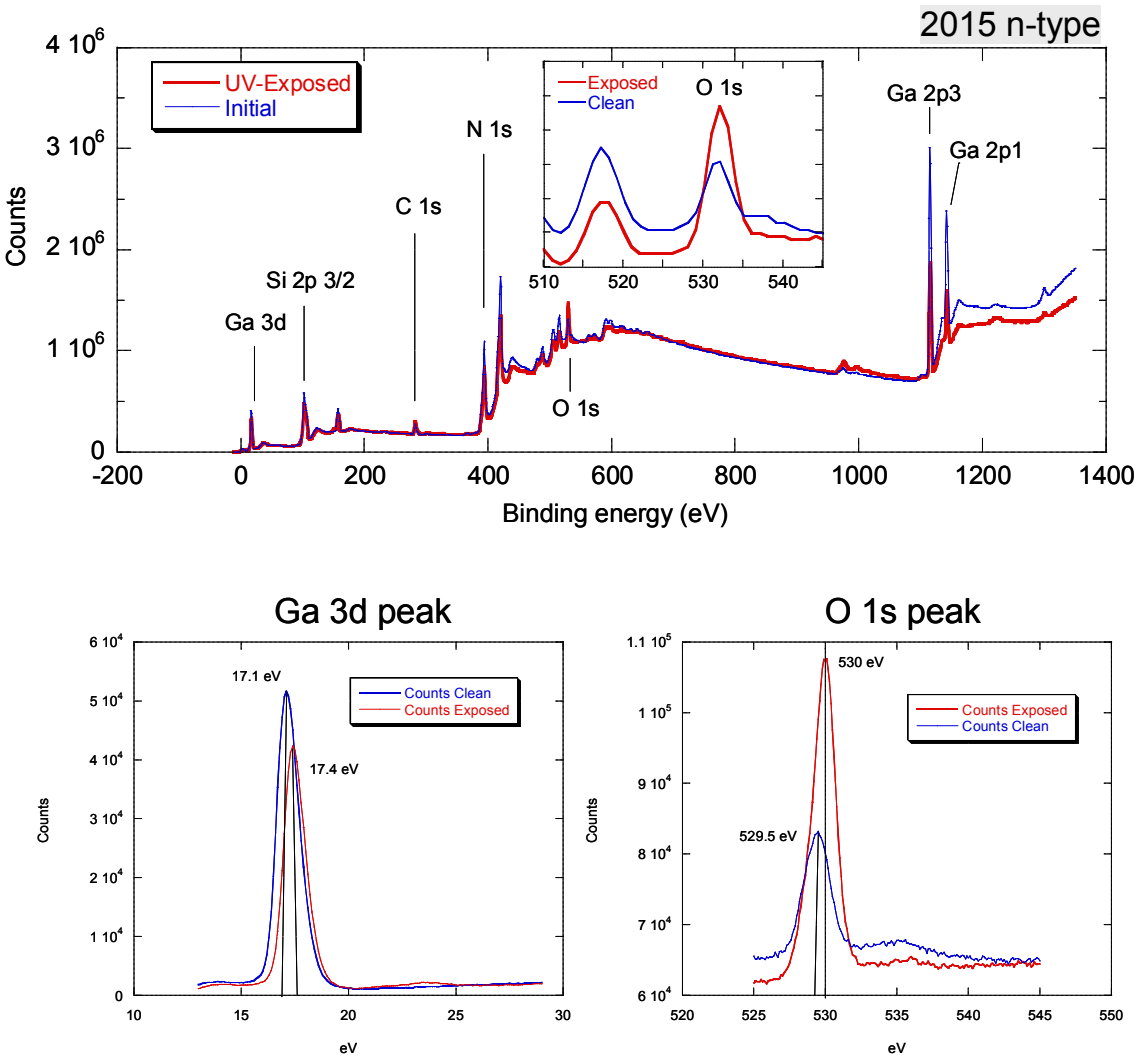

Fig. 3.3: XPS survey of clean and UV-exposed n-type 2015 sample (a). Detail of Ga 3d peak (b) and detail of oxygen peak (c) shown below

www.manaraa.com

Chapter 4: Band Diagram Interpretation

4.1: Band Diagrams for MOS system

An analogy can be drawn between the standard metal-oxide-semiconductor (MOS) system and charging the GaN surface with a conducting AFM tip in the presence of a surface oxide. In a typical MOS system, an oxide layer is sandwiched between a metal electrode and a semiconductor, and the components are electronically connected. Depending on the type of semiconductor used, a MOS may be either n-MOS or a p-MOS by employing n-type or p-type semiconductor materials, respectively. The distribution of electronic charge in a MOS system is modulated by applying various voltages to the metal electrode, which is referred to as the gate in a field-effect transistor configuration (MOS-FET). Generally, the convention is that forward-biasing occurs for n-MOS when $V_G > 0$, and reverse bias occurs for $V_G < 0$. It should be noted, however, that in the GaN surface charging experiments presented here, the bias voltage is applied to the semiconductor sample and the metal tip is grounded. Forward- and reverse-biased surface charging and the resultant surface potential behavior can be interpreted by analogous behaviors of a MOS system.

To interpret charging of the GaN system, certain modes of MOS operation must first be addressed. The forward-bias mode of MOS operation causes majority carriers to accumulate at the semiconductor/oxide interface, which for the n-type sample occurs when a negative sample voltage V_S is applied. An energy band diagram for an n-type sample after forward-biasing is depicted in Fig. 4.1a. The applied voltage creates a "sheet charge" of electron accumulation at the oxide-semiconductor interface, resulting in decreased band bending at the interface. The extent of band bending is determined by contributions from the intrinsic band bending Φ_0 and from the applied voltage. In the case of the GaN system, we do not expect a perfectly insulating surface oxide layer and there may be traps at the oxide interface which become filled during biasing. In fact, the presence of a thick oxide, e.g., after UV exposure, appears to be critical to the accumulation of surface charge under forward-bias conditions.

www.manaraa.com

Conversely, the reverse-bias mode of a MOS system is achieved by applying a positive voltage V_S to the sample. As the applied V_S voltage increases in magnitude, the extent of band bending increases and the width of the depletion zone at the semiconductor interface increases (Fig. 4.1c). For the GaN system, this bias condition can result in a substantial charging of the surface and resultant band bending.

4.2: Band Diagrams for the GaN System

Energy band diagrams will be presented for the GaN system which are consistent with SKPM measurements taken immediately after charging with contact AFM. Although some of the attributes of the system are not explicitly known, e.g., properties of the surface oxide layer, qualitative descriptions of associated energy band diagrams is indeed possible for various applied sample biases. Typical values for known quantities include: the work function of the platinum-coated AFM tip of $\varphi_m = 5.1$ eV,[23] the electron affinity for GaN of $\chi_s = 4.1$,[24] and the band gap for GaN of $E_G = 3.4$ eV.[1] The surface oxide will be assumed to be an amorphous GaO compound with an approximate band gap of 5 eV[25] and an electron affinity of $\chi_{ox} = 2.6$ eV.[26] The thickness of the oxide is another important consideration, and we will assume a thickness on the order of 1 to 2 nm.

An equilibrium band diagram before charging for n-type GaN is shown in Fig. 4.2 with an intrinsic band bending Φ_S of approximately 1 eV.[27] This band diagram will change as a function of charging, where the change of the contact potential ΔV_{CP} can be measured by SKPM, as discussed in previous chapters. After charging under forward-bias conditions, only a small, positive ΔV_{CP} value of 0.1 to 0.3 V is observed experimentally (see Fig. 2.1). This result would be consistent with a band diagram having a small decrease in the band bending Φ_S and a small voltage drop (~0.1 V) across the thin oxide layer, as shown in Fig. 4.3. It should be noted that the breakdown electric field of the oxide layer prevents any substantial voltage drop across it. The fact that charging under forward-bias conditions is usually only possible after growing a thicker oxide layer indicates that charge trapping in the oxide is an important mechanism.

www.manaraa.com

In contrast, charging under reverse-bias conditions results in a relatively large, negative ΔV_{CP} value of –1 to –3 V. This behavior must primarily result from a large increase in band bending, because only a small voltage drop can occur across the oxide layer. The increased band bending leads to a substantial increase in width of the depletion region W given by:

$$W = \sqrt{\frac{2\Phi\varepsilon\varepsilon_0}{q^2 N_D}}$$

where n_s is the surface charge density, N_D is the concentration of uncompensated shallow donors, ε is the dielectric constant for GaN, ε_0 is the permittivity of vacuum, and q is the electron charge. In a typical charging experiment, a four-fold increase of band bending (e.g., from Φ_S = 1 eV to 4 eV) would result in a doubling of the depletion width.

Charging of p-type GaN should result in analogous band diagrams. The uncharged, equilibrium band diagram (Fig. 4.5) is also expected to have an initial band bending Φ_S of approximately 1 eV. After charging under forward-bias conditions, we again experimentally observe a small ΔV_{CP} value of –0.1 to –0.3 V, indicating only a small decrease in band bending Φ_S and a small voltage drop across the oxide layer (Fig. 4.6). Similar to n-type GaN, the presence of a thicker oxide is necessary to produce surface charging under this bias condition. In the case of reverse-bias charging, p-type GaN produces a large ΔV_{CP} value of a few eV that can only be explained by an increase in band bending of approximately the same magnitude (Fig. 4.7).

The band diagrams presented here are consistent with experimental SKPM data, but the voltage drop across the oxide layer and its important role in the case of forward-bias charging still requires further investigation.

4.3: Conclusions

We have observed several charging phenomena that exist on GaN surfaces. The ability to locally charge both n-type and p-type GaN surfaces with both polarities has been demonstrated here for the first time. However, forward-bias charging is usually only possible

www.manaraa.com

after the surface has been exposed to either ambient humidity or UV illumination. There is an observed asymmetry for ΔV_{CP} values, where charging under reverse-bias conditions yields higher values. Interestingly, this asymmetry may be used to characterize an unknown surface as either p-type or n-type. In the case of p-type surfaces, we have found that Hall Effect measurements can sometimes indicate n-type doping due to the presence of an n-doped layer at the substrate interface. Therefore, one must be careful when distinguishing whether a sample should be considered as n-type or p-type with regard to surface behavior.

The ability to pattern the GaN surface with localized charge could be of interest. As was demonstrated in Chapter 2, a rudimentary read-write-erase capability is possible. We have observed a "bit" resolution for positive charge of 500 nm, but higher resolution is likely possible. This capability could potentially be used to store information on the GaN surface, although charge decay and sensitivity to environmental factors would likely make practical application of this technology unlikely. There may also be a possibility to implement this charge patterning technique as a template for deposition and/or nanostructure growth. Ionized precursors may preferentially deposit on locally charged regions and therefore nucleate growth in such regions. Issues to address would include preferential deposition, temperature effects, and scalability of patterning.

The decay of the deposited surface charge has also been investigated under dark conditions. A comparison of the decay behavior for positive and negative surface charge on both n-type and p-type surfaces illustrates a faster decay rate for surface-to-bulk electron transfer vs. bulk-to-surface. This behavior results in positive surface charge persisting for longer time periods on both n- and p-type samples. Time-dependent data also indicate that charge decays faster at higher temperatures, which would support a thermionic mechanism of electron transfer over a surface barrier. An analytical model of this behavior is beyond the scope of this thesis, but work will continue on this project in the research group. The dependence of the decay behavior on the nature of the surface oxide layer, surface defects, and other variables complicates the construction of such a model. As we observed, extended

www.manaraa.com

UV treatment causes significant lateral diffusion of negative surface charge, indicating that a grown surface oxide is significantly more conductive than the native oxide.

As shown in the previous section, energy band diagrams suggest that the oxide layer plays a significant role in forward biasing experiments, while in reverse bias, induced band bending is likely to be the dominant mechanism. Future consideration of band diagrams may include improved estimates of oxide layer properties and band bending values. This work demonstrates that consideration of surface layers from adsorbed oxygen or water species must be accounted for in order to correctly characterize surface properties.

www.manaraa.com

Chapter 4 Figures

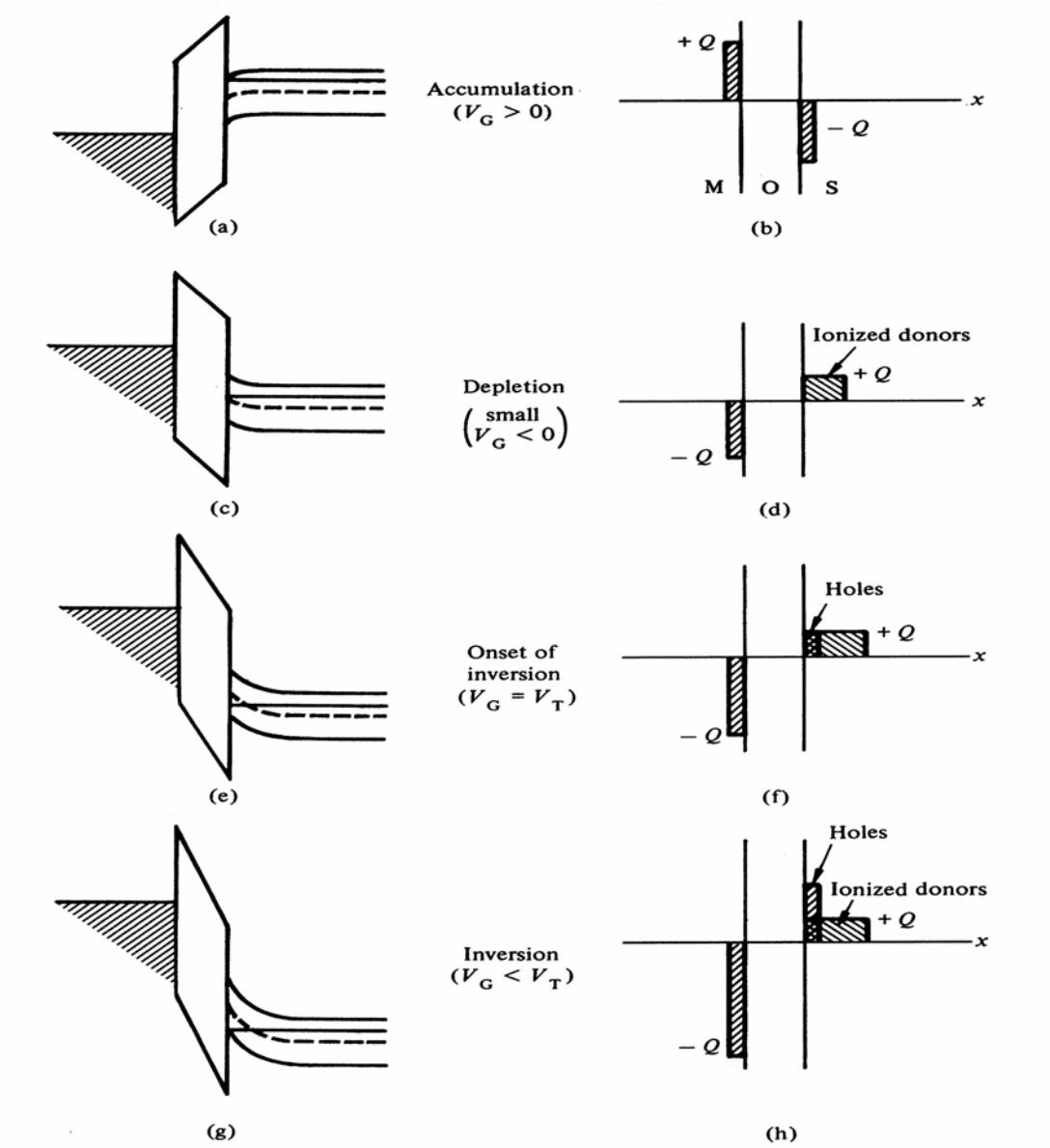

Figure 16.5

Fig. 4.1: n-MOS diagram for various modes of operation.[28]

www.manaraa.com

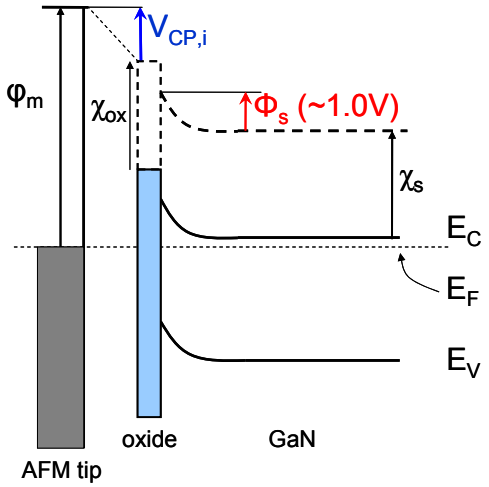

Fig. 4.2: n-type band diagram under equilibrium conditions

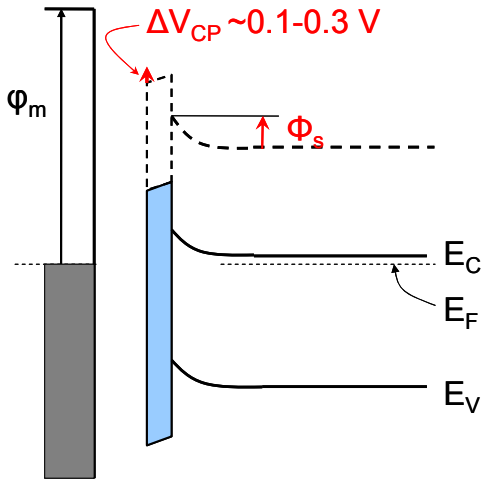

Fig. 4.3: n-type band diagram after charging under forward bias conditions.

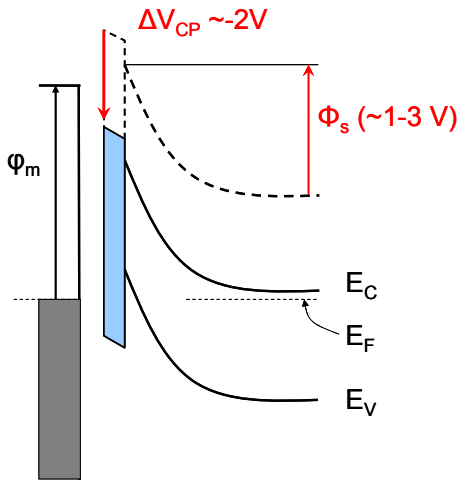

Fig. 4.4: n-type band diagram after charging under reverse bias conditions.

www.manaraa.com

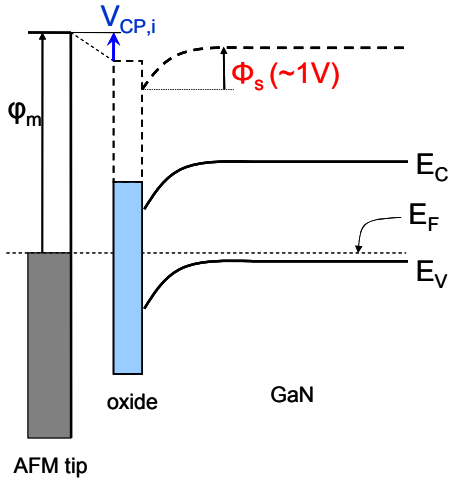

Fig. 4.5: p-type band diagram under equilibrium conditions

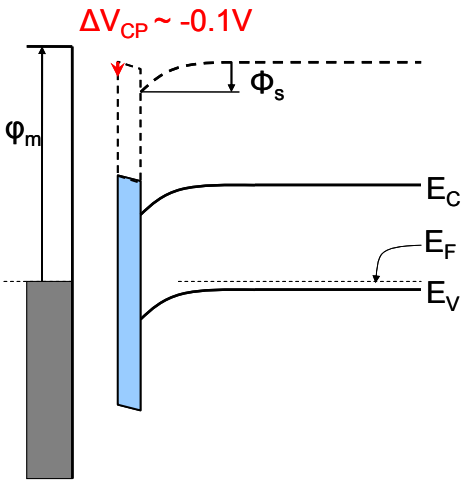

Fig. 4.6: p-type band diagram after charging under forward bias conditions.

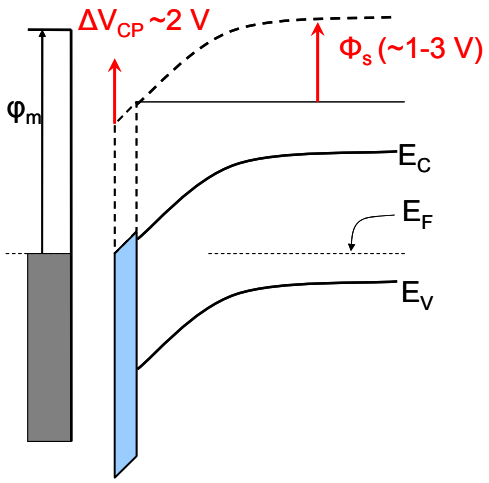

Fig. 4.7: p-type band diagram after charging under reverse bias conditions.

www.manaraa.com

References

[1] H. Morkoç *Nitride Semiconductors and Devices*. Berlin: Springer-Verlag (1999).

[2] F. Raab, *et al. IEEE Transactions on Microwave Theory and Techniques* **50,** 3 (2002).

[3] R.D. Dupuis, *IEEE J. Quant. Electr.* **WE-23** 651-657 (1987).

[4] S. Sabuktagin, Y.T. Moon, S. Dogan, A.A. Baski, and H. Morkoç, *IEEE Electr. Dev.* **50** (4), 886 (2003).

[5] G. Binnig, C. Gerber, and C.F. Quate, *Phys. Rev. Lett.* **56**, 930-933 (1986).

[6] G. Binnig and H. Rohrer, *IBM Journal of Research and Development* **30**, 4 (1986).

[7] Y. Martin and K. Wickramasinghe, *Appl. Phys. Lett.* **50**, 1455–1457 (1987).

[8] F.J. Rubio-Sierra *et al., Adv. Eng. Mat.***7**, 4 193-196 (2005).

[9] J.E. Stern *et al., Appl. Phys. Lett* **53**, 26 (1988).

[10] J.C Moore, M.A. Reshchikov, J.E. Ortiz, J. Xie, H. Morkoç and A.A. Baski, *Proc. Of the SPIE* **6894,** 68940B1-9 (2008).

[11] J.D. Ferguson, M.A. Foussekis, M.D. Ruchala, J.C Moore, M.A Reshikov and A.A. Baski, *MRS Proc.***1202** 1202-I04-01 (2009).

[12] M.A. Foussekis, J.D. Ferguson, X. Ni, H. Morkoç, M.A. Reshchikov, and A.A. Baski, *Proc. of the SPIE* **7602** (2010).

[13] Veeco ICON AFM used for all data acquisition.

[14] Conductive AFM canitilevers are Mikromasch^{TM} NSC-14 Ti-Pt metallized (k_{tip}~ 5 N/m).

[15] M. Nonnenmacher, M.P. O'Boyle, and H.K. Wickramasinghe, *Appl. Phys. Lett.* **58**, 2921 (1991).

[16] S. Barbet *et al.*, *Appl. Phys. Lett.* **93** 212107 (2008).

[17] G. Ertl and J. Küppers, *Monographs in Modern Chemistry* **4** (1974).

[18] Q. Xu and J.W.P. Hsu, *J. Appl. Phys.* **85**, 2465 (1995).

[19] C.H. Lei, A. Das, M. Elliot, and J.E. Macdonald, *Nanotechnology* **15**, 627-634 (2004).

[20] D.C. Look and R.J. Molnar, *Appl. Phys. Lett,* **70** 3377 (1997).

[21] M.A. Foussekis, A.A. Baski, and M.A. Reshchikov, *Appl. Phys. Lett.* **94**, 162116 (2009).

[22] Thermo-Fisher ESCALAB 250 with 1486.6 eV Al Kα source.

www.manaraa.com

[23] R.C. Weast, *ed.* CRC Handbook of Chemistry and Physics, 65 ed. Boca Raton, Fl: CRC Press (1985).

[24] V. Bougrov, M. Levinshtein, S. Rumyantsev, and A. Zubrilov, Properties of Advanced SemiconductorMaterials GaN, AlN, InN, BN, SiC, SiGe New York: John Wiley & Sons, Inc., pp. 1-30 (2001).

[25] G. Sinha et al., *J. Phys. Cond. Mat.***18** (2006).

[26] G. Meloni et al., *J. Chem Phys* **122,** 074317 (2005).

[27] M.A. Reshchikov, M.A. Foussekis, and A.A. Baski, *J. App. Phys.* **107** (2010), (in press)

[28] R.F. Pierret Semiconductor Device Fundamentals New York: John Wiley and Sons. Ch. 16 (1996)

www.manaraa.com